Electronic Supplementary Material

Cobalt-nanoparticle catalysts derived from zeolitic imidazolate framework@MXene composites for efficient oxidative self-coupling of benzylamines

Jie Chen*, Mingyuan Jian*, Deqiong Xie, Kecan Dou, De-Li Chen, Weidong Zhu **(✉)**, Fumin Zhang **(✉)**

Key Laboratory of the Ministry of Education for Advanced Catalysis Materials, Institute of Physical Chemistry, Zhejiang Normal University, Jinhua 321004, China

E-mails: weidongzhu@zjnu.cn (Zhu W); zhangfumin@zjnu.edu.cn (Zhang F)

* These authors contributed equally to this work.

1 Experimental

1.1 Chemicals

Ti_3AlC_2 (98%, 200 mesh) powders were obtained from Meryer Chemical Technology Co., Ltd. Cobalt nitrate hexahydrate (99.99%, $Co(NO_3)_2·6H_2O$), 2–methylimidazole (98%), decane (98%), 4–methoxybenzylamine (98%), benzylamine (99%), 2–methylbenzylamine (98%), 3–methylbenzylamine (>97%), 4–tert–butylbenzylamine (≥98%), 3–(aminomethyl) pyridine(>99%), 2–furylmethylamine (99%), dibenzylamine (98%), 1,2,3,4–tetrahydroisoquinoline (≥95%), aniline (99.5%), 4–(trifluoromethyl)benzylamine (98%), and 2,6–di–tert–butyl–4–methylphenol (>99.5%, BHT) were purchased from Aladdin Industrial Inc. Hydrofluoric acid (≥40%, HF), zinc nitrate hexahydrate (≥98%, $Zn(NO_3)_2·6H_2O$), cetyltrimethylammounium bromide (CTAB), methanol, toluene, acetonitrile, *N*, *N*–dimethylformamide, ethanol, heptane, acetone, aqua fortis (68%, HNO_3), hydrogen peroxide (30%, H_2O_2), and hydrochloric acid (36.0~38.0%, HCl) were supplied by Sinopharm

Chemical Reagent Co., Ltd. 2–Thiophenemethylamine (≥99%), 4–fluorobenzylamine (99.4%), 4–chlorobenzylamine (≥99%), 4–bromobenzylamine (≥98%), and 4–methylbenzylamine (≥99%) were supplied by Bide Pharmatech Ltd. All chemicals were used without additional purification.

1.2 Catalyst characterization

Powder X–ray diffraction (XRD) patterns were obtained on a Philips PW3040/60 diffractometer using Cu Kα radiation (λ=0.1541 nm, 40 kV, 30 mA).

N_2 adsorption–desorption isotherms were measured at 77 K on a Micromeritics ASAP 2020 instrument. The samples were outgassed under vacuum at 423 K for 12 h before adsorption measurement. The specific surface areas of the investigated samples were calculated using the multiple–point Brunauer–Emmett–Teller (BET) method in the relative pressure range of P/P_0 = 0.05–0.30 and the total pore volumes were determined at a relative pressure of 0.95.

The morphology of the samples was obtained by field emission SEM on a scanning electron microscope (a Hitachi S–4800 microscope) and TEM on a transmission electron microscope (JEM2100F, JEOL, Japan) working at 200 kV.

Raman spectroscopy was performed on the InVia–Renishaw instrument with the laser source at 532 nm.

X–ray photoelectron spectroscopy (XPS) data were collected on an ESCALAB250 electron spectrometer from VG Scientific using 300 W Al–Kα radiation. The XPS data were internally calibrated, fixing the binding energy of C 1s at 284.8 eV.

The concentrations of Co metal species in the various samples were determined using an IRIS Intrepid II XSP inductively coupled plasma–atomic emission spectrometer (ICP–AES). The sample dissolution process proceeded as follows: 20 mg of the test samples were placed into a 50 mL Teflon−lined stainless steel autoclave reactor, and 8 mL of aqua regia and 2 mL

of HF were added and mixed thoroughly. The mixture was then heated in an oven at 453 K for 12 hours, and after cooling, the fully dissolved sample was transferred to a 50 mL volumetric flask and diluted to 50 mL with deionized water.

1.3 Catalyst preparation

1.3.1 Synthesis of Co–ZIF@MXene, ZnCo(1:1)–ZIF@MXene, and Zn–ZIF@MXene Composites

Co–ZIF@MXene, ZnCo(1:1)–ZIF@MXene, and Zn–ZIF@MXene were synthesized using the same method as ZnCo(19:1)–ZIF@MXene, but with 40 mL of methanol solution containing 2 mmol $Co(NO_3)_2 \cdot 6H_2O$ or $Zn(NO_3)_2 \cdot 6H_2O$ or their mixture of Zn/Co in a 1:1 molar ratios, respectively.

1.3.2 Fabrication of Co–$NPs_{(21.1)}$/NC@MXene, Co–$NPs_{(16.2)}$/NC@MXene, and NC@MXene

Co–$NPs_{(21.1)}$/NC@MXene, Co–$NPs_{(16.2)}$/NC@MXene and NC@MXene were synthesized similarly to Co–$NPs_{(8.6)}$/NC@MXene, using Co–ZIF@MXene, ZnCo–ZIF(1:1)@MXene, and Zn–ZIF@MXene as precursors, respectively.

1.3.3 Synthesis of ZnCo(19:1)–ZIF and Co–NC

The ZnCo(19:1)–ZIF was synthesized using the same method as ZnCo(19:1)–ZIF@MXene, but without the addition of Ti_3C_2 MXene, and with a starting Zn/Co molar ratio of 19:1. Subsequently, Co–NC was prepared by subjecting the ZnCo(19:1)–ZIF to the same heat treatment as Co–$NPs_{(8.6)}$/NC@MXene.

1.3.4 Preparation of MXene–1173

200 mg of Ti_3C_2 MXene underwent complete carbonization in a tubular furnace using identical pyrolysis conditions to Co–$NPs_{(8.6)}$/NC@MXene, resulting in the formation of MXene–1173.

1.4 Catalytic performance test

Kinetic research on the oxidative coupling of 4−methoxybenzylamine was conducted to determine the reaction's kinetics over Co−NPs$_{(8.6)}$/NC@MXene. The reactor temperature was adjusted to desired values (363 K, 373 K, and 383 K), and the reaction at each temperature was modeled using pseudo−first−order kinetics. The value of −ln(1−x) was calculated based on the conversion of 4−methoxybenzylamine (x) to generate a plot of −ln(1−x) against reaction time in minutes. The pseudo−first−order rate constants (k) were then obtained from the slope of the plot. The activation energy (E_a) for the reaction was estimated using the Arrhenius equation, with data points controlled below a 20% conversion of 4−methoxybenzylamine. The Arrhenius factor (A), activation energy (E_a), and rate constant (k) at temperature T (in Kelvin) were used in the equation.

Table S1 Textural properties and cobalt content of the various catalysts investigated.

Entry	Catalyst	Co/wt.%[a)]	S_{BET}/m^2/g[b)]	V_{total}/cm^3/g[c)]
1	NC@MXene	—	163.1	0.12
2	Co–NPs$_{(8.6)}$/NC@MXene	0.77	429.2	0.40
3	Co–NPs$_{(16.2)}$/NC@MXene	13.96	107.7	0.13
4	Co–NPs$_{(21.1)}$/NC@MXene	21.01	64.8	0.12
5	Co–NC	2.21	742.4	0.93
6	MXene–1173	—	28.1	0.11

a) By ICP−AES analysis. b) By BET method. c) By *t*−plot method.

Table S2 Total N contents and relative contents of the different N species in the prepared catalysts.

Catalyst	Total N/atom%	Relative contents of different N species/area%				
		Ti N	Pyridinic N	Pyrrolic N	Graphitic N	N Oxide
NC@MXene	9.20	6.8	19.5	37.0	28.3	8.4
Co–NPs$_{(8.6)}$/NC@MXene	6.52	1.4	43.4	15.9	30.4	8.9
Co–NPs$_{(16.2)}$/NC@MXene	5.80	23.2	27.4	25.7	14.3	9.4
Co–NPs$_{(21.1)}$/NC@MXene	5.37	16.5	28.2	31.7	13.6	10.0
Co–NPs/NC	6.36	—	37.3	18.4	28.1	16.2

Table S3 Optimization of the reaction conditions for oxidative self–coupling.

Entry	Solvent	Catalyst amount/mg	Conv./%[a)]	Sel./%[a)]
1	Toluene	15	62.1	98.8
2	DMF	15	97.1	71.6
3	Heptane	15	57.8	96.8
4	Decane	15	97.4	97.9
5	Ethanol	15	20.0	97.6
6	Acetonitrile	15	69.1	99.1
7	Decane	5	60.0	96.0
8	Decane	25	99.9	93.1
9[b)]	Decane	15	63.9	98.8
10[c)]	Decane	15	36.9	99.9

Reaction conditions: 4–methoxybenzylamine (0.5 mmol), Co–$NPs_{(8.6)}$/NC@MXene, solvent (3 mL), 1 atm O_2, 383 K, 8 h. a) Determined through GC using diphenyl as the internal standard and confirmed by GC−MS. b) Reaction under Air atmosphere. c) Reaction under 1 bar N_2.

Table S4 Comparison of catalytic oxidative coupling of 4–methoxybenzylamine over different catalysts.

Entey	Catalyst	Yield/%	TOF/h^{-1}[a)]	Ref.
1	Co–$NPs_{(8.6)}$/NC@MXene	95.4	30.41	This work
2	meso–Cs/MnO_x	95.0	0.68	[s1]
3	α–MnO_2	94.1	2.35	[s2]

4	$Fe_2Mn(\mu_3–O)(BPTC)_2(DMF)_2(H_2O)$	80.0	7.33	[s3]
5	meso–MoO_x–300	97.0	1.74	[s4]
6	$[Co(L)_2]_2[Mo_6O_{19}]$	78.0	0.27	[s5]
7	Co–NC/SiO_2	99.0	0.52	[s6]
8	acac–MnO_x	88.7	0.63	[s7]
9	Co–N/C–800	99.0	13.75	[s8]
10	Cu^I/$\mathbf{1}_{ox}$	95.0	47.5	[s9]
11	$[Et_3NH]_2[Ru(dipic)Cl_3]$	99.0	8.25	[s10]

a) TOF: turnover frequency.

References

s1. Biswas S, Dutta B, Mullick K, Kuo C H, Poyraz A S, Suib S L. Aerobic oxidation of amines to imines by cesium–promoted mesoporous manganese oxide. ACS Catalysis, 2015, 5(7): 4394–4403

s2. Zhang Z, Wang F, Wang M, Xu S, Chen H, Zhang C, Xu J. tert–Butyl hydroperoxide (TBHP)–mediated oxidative self–coupling of amines to imines over a α–MnO_2 catalyst. Green Chemistry, 2014, 16(5): 2523–2527

s3. Wang Y X, Wang H M, Meng P, Song D X, Qi Z, Zhang X M. $Fe_2Mn(\mu_3–O)(COO)_6$ cluster based stable MOF for oxidative coupling of amines via heterometallic synergy. Chinese Journal of Chemistry, 2021, 39(11): 2983–2989

s4. Shubhashish S, Khanna H S, Achola L A, Amin A S, Willis W S, Suib S L. Selective oxidative coupling of amines using mesoporous MoO_x catalysts. ACS Applied Nano Materials, 2021, 4(2): 2086–2097

s5. Zhao M, Li J, Xing C, Han Q, Ma L, Li M. A new cobalt(III)/$[Mo_6O_{19}]^{2-}$ heterogeneous catalyst for promoting the oxidative coupling of amines to imines. Catalysis Letters, 2020, 150(3): 753–761

s6. Zhang C, Zhao P, Zhang Z, Zhang J, Yang P, Gao P, Gao J, Liu D. Co–N–C supported on SiO_2: a facile, efficient catalyst for aerobic oxidation of amines to imines. RSC Advances, 2017, 7(75): 47366–47372

s7. Jia X, Ma J, Xia F, Gao M, Gao J, Xu J. Switching acidity on manganese oxide catalyst with acetylacetones for selectivity–tunable amines oxidation. Nature Communications, 2019, 10: 2338

s8. Cui X, Li W, Junge K, Fei Z, Beller M, Dyson P J. Selective acceptorless dehydrogenation of primary amines to imines by core–shell cobalt nanoparticles. Angewandte Chemie International Edition, 2020, 59(19): 7501–7507

s9. Largeron M, Fleury M B. A biologically inspired Cu^{I}/topaquinone–like Co–catalytic system for the highly atom–economical aerobic oxidation of primary amines to imines. Angewandte Chemie International Edition, 2012, 51(22): 5409–5412

s10. Zhang Y, Lu F, Huang R, Zhang H, Zhao J. Aerobic oxidation of amines to imines catalyzed by a ruthenium complex under solvent–free conditions. Catalysis Communications, 2016, 81: 10–13

Table S5 Kinetic parameters of oxidative coupling of 4–methoxybenzylamine catalyzed by Co–NPs$_{(8.6)}$/NC@MXene.

***T* (K)**	***k*/min^{-1}**	***E*$_a$/kJ/mol**
363	4.7×10^{-3}	
373	7.2×10^{-3}	48.1 ± 1.7
383	10.6×10^{-3}	

Reaction conditions: 4–methoxybenzylamine (0.5 mmol), Co–NPs$_{(8.6)}$/NC@MXene (15 mg), decane (3 mL), 1 atm O_2.

Table S6 Effect of additive on oxidation of 4–methoxybenzylamine to imine in the presence of Co–NPs$_{(8.6)}$/NC@MXene.

Entry	**Additive**	**Conv./%[a)]**	**Sel./%[a)]**
1	—	45.2	96.5
2[b)]	H_2O	45.0	97.0
3[c)]	3 Å molecular sieve	36.1	98.2
4[d)]	BHT	44.7	96.9

Reaction conditions: 4–methoxybenzylamine (0.5 mmol), catalyst (15 mg), decane (3 mL), 1 atm O_2, 383 K, 1 h. a) Determined through GC using diphenyl as the internal standard and confirmed by GC−MS. b) Added 1 mmol. c) Added 0.15 g. d) Added 0.2 mmol.

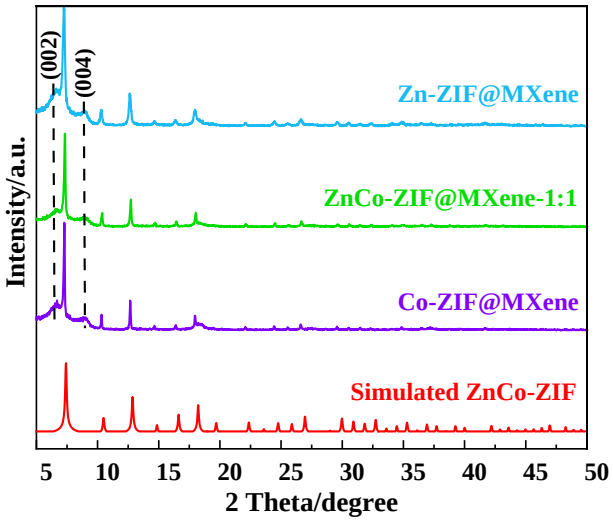

Fig. S1 The XRD patterns for Co–ZIF@MXene, ZnCo(1:1)–ZIF@MXene and Zn–ZIF@MXene.

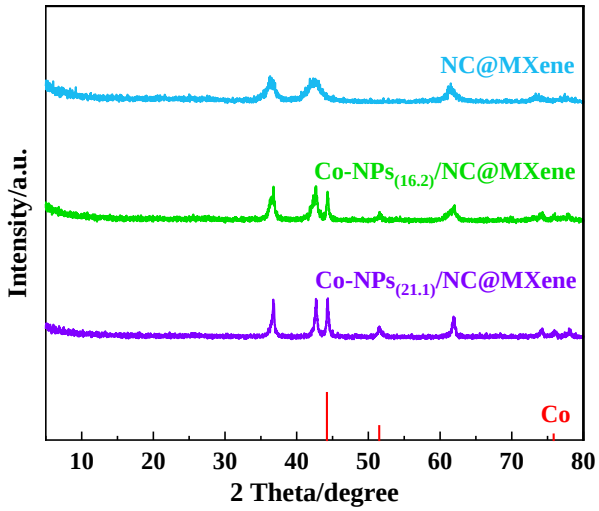

Fig. S2 The XRD patterns for Co–$NPs_{(21.1)}$/NC@MXene, Co–$NPs_{(16.2)}$/NC@MXene and NC@MXene.

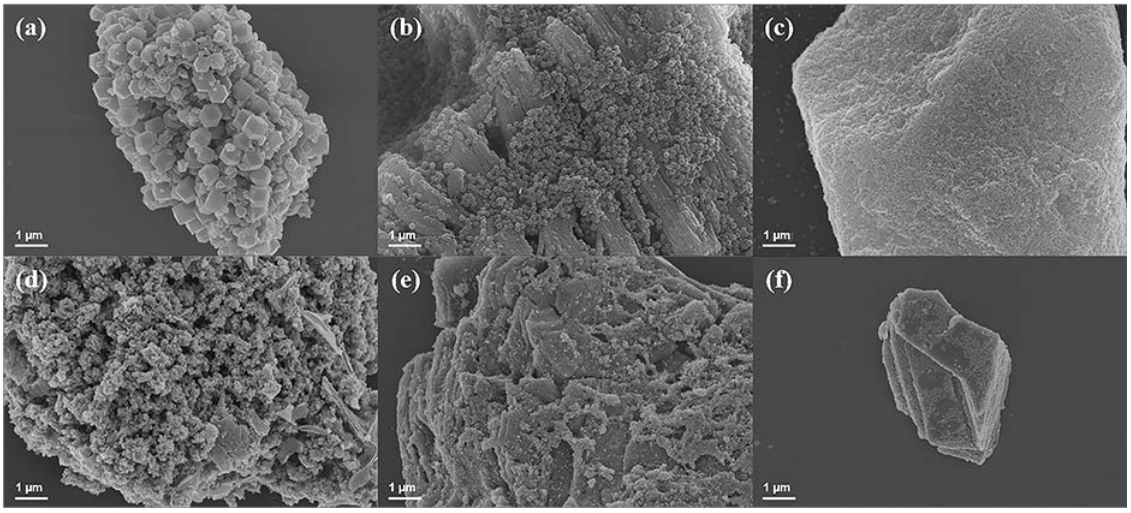

Fig. S3 SEM images of (a) Co–ZIF@MXene (b) ZnCo(1:1)–ZIF@MXene (c) Zn–ZIF@MXene (d) Co–NPs$_{(21.1)}$/NC@MXene (e) Co–NPs$_{(16.2)}$/NC@MXene and (f) NC@MXene.

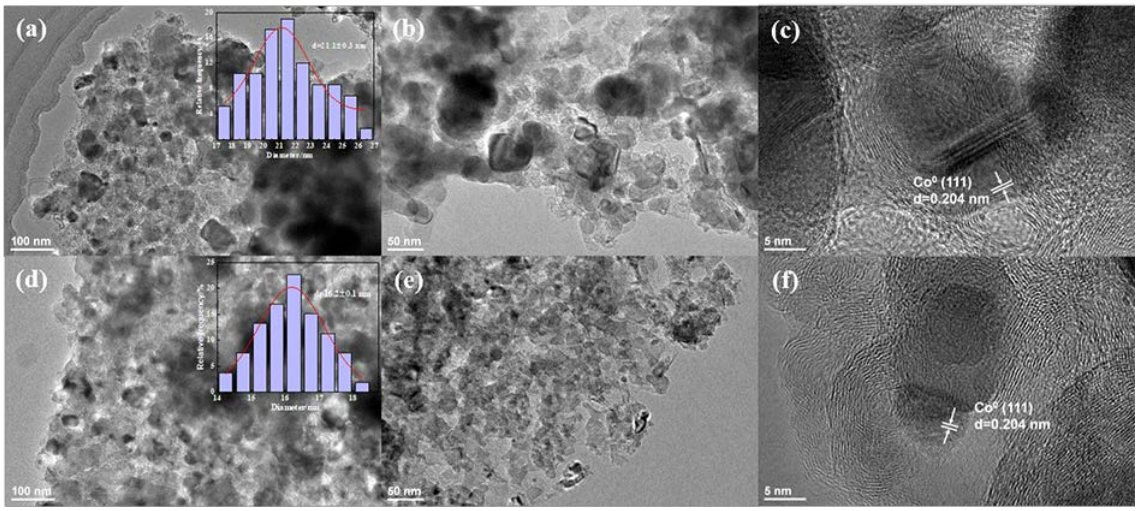

Fig. S4 TEM and HRTEM images of (a, b, c) Co–NPs$_{(21.1)}$/NC@MXene and (d, e, f) Co–NPs$_{(16.2)}$/NC@MXene.

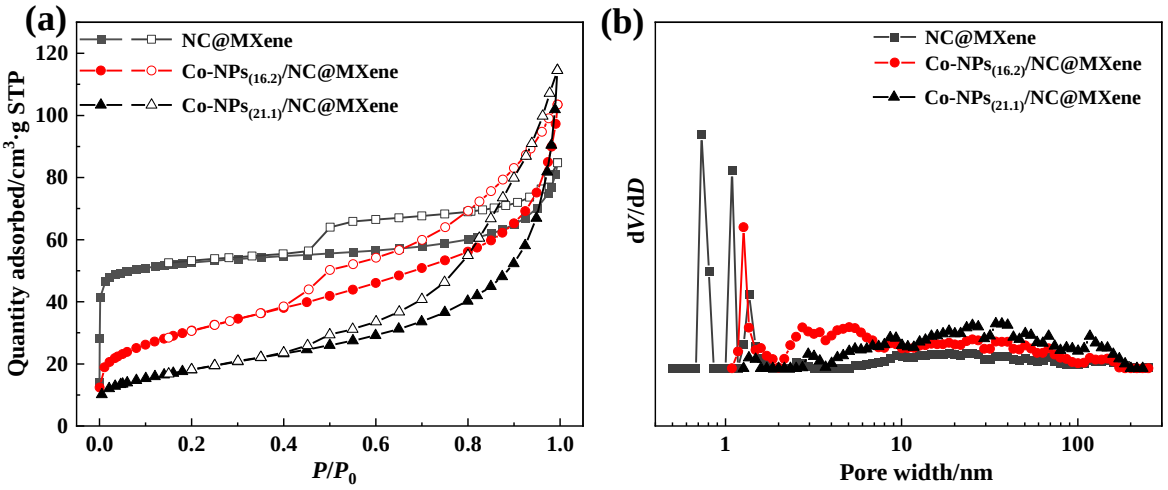

Fig. S5 (a) N_2 adsorption–desorption isotherms and (b) pore size distribution of synthesized Co–NPs$_{(21.1)}$/NC@MXene, Co–NPs$_{(16.2)}$/NC@MXene and NC@MXene.

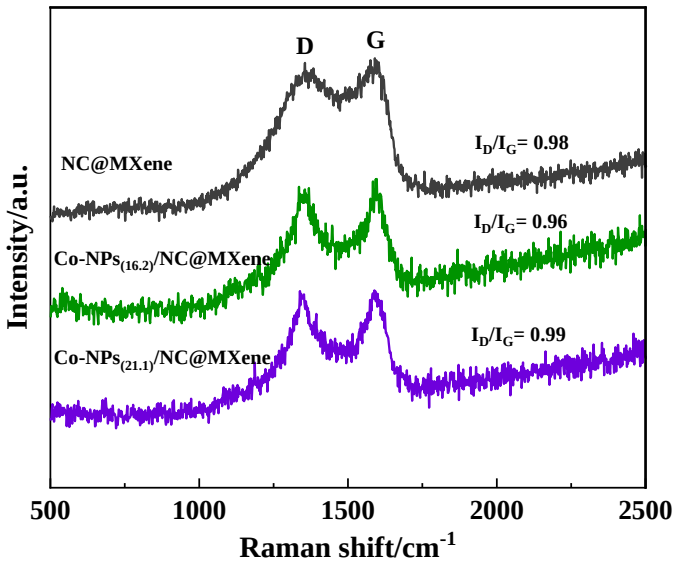

Fig. S6 Raman spectra of Co–NPs$_{(21.1)}$/NC@MXene, Co–NPs$_{(16.2)}$/NC@MXene and NC@MXene.

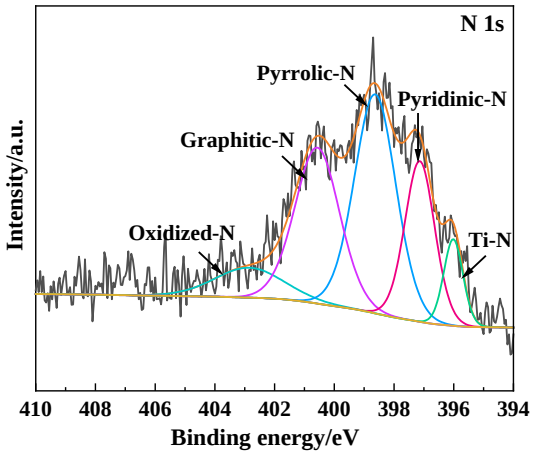

Fig. S7 XPS spectra of N 1s for NC@/MXene.

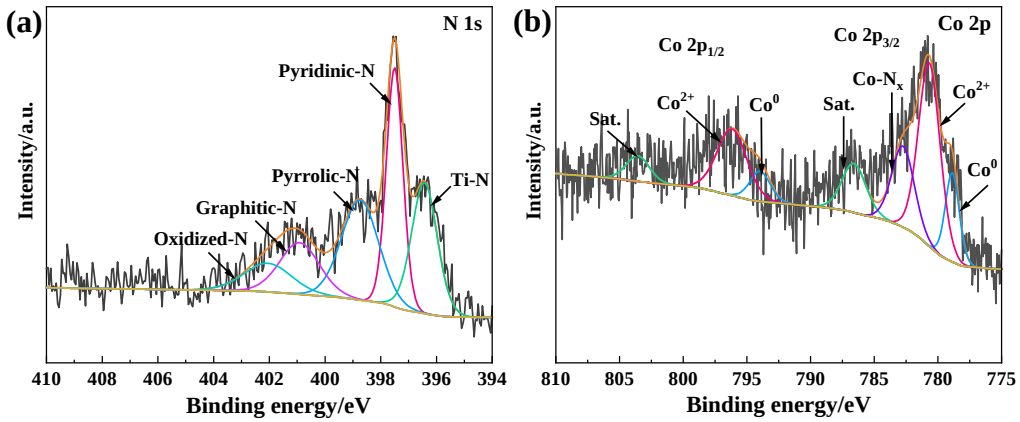

Fig. S8 XPS spectra of (a) N 1s and (b) Co 2p for Co–NPs$_{(16.2)}$/NC@MXene.

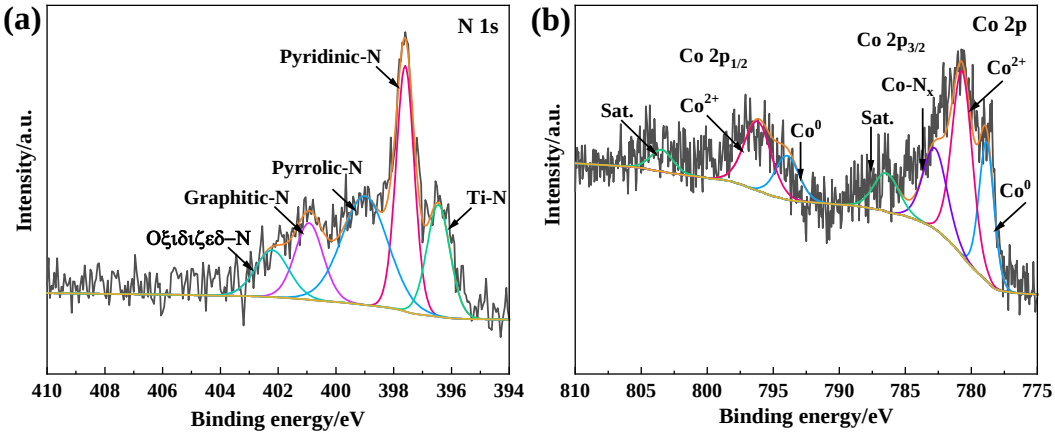

Fig. S9 XPS spectra of (a) N 1s and (b) Co 2p for Co–NPs$_{(21.1)}$/NC@MXene.

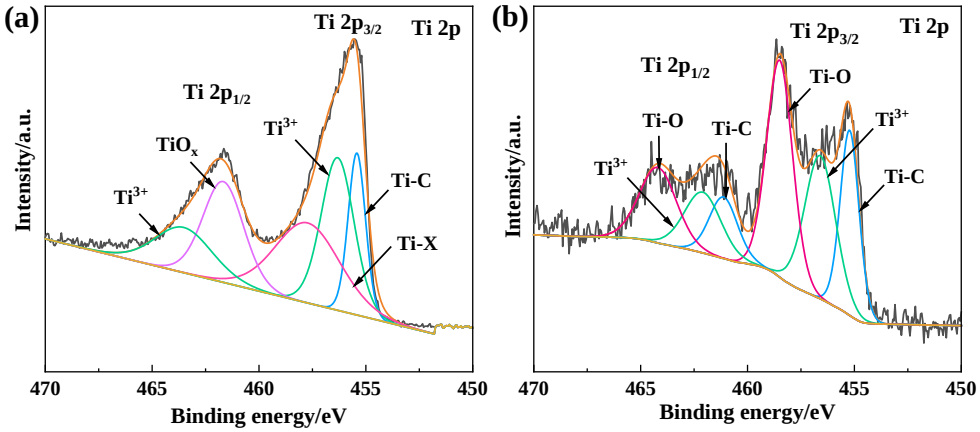

Fig. S10 XPS spectra of Ti 2p of (a) Ti_3C_2 MXene and (b) Co–$NPs_{(8.6)}$/NC@MXene.

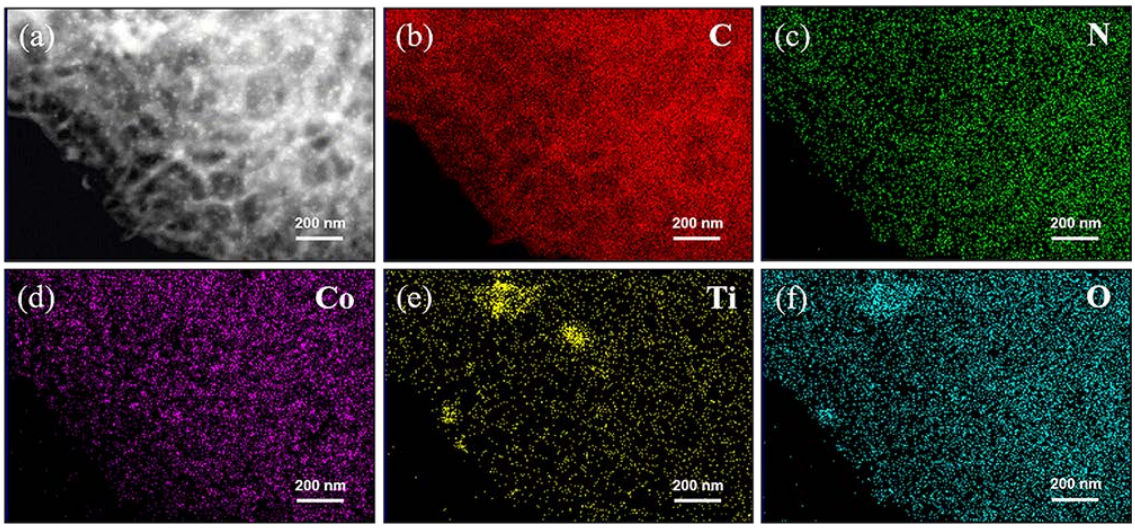

Fig. S11 Energy-dispersive X-ray spectroscopy mapping of Co–$NPs_{(8.6)}$/NC@MXene.

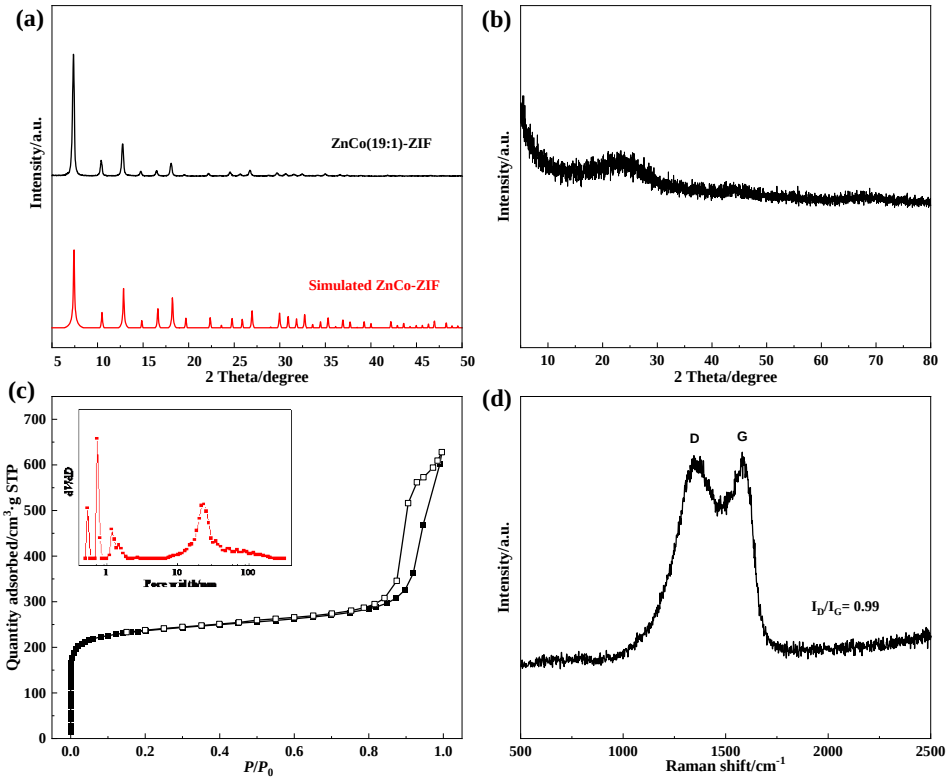

Fig. S12 (a) XRD patterns of ZnCo(19:1)–ZIF. (b) XRD patterns, (c) N_2 adsorption–desorption isotherms and pore size distribution and (d) Raman spectra of Co–NC.

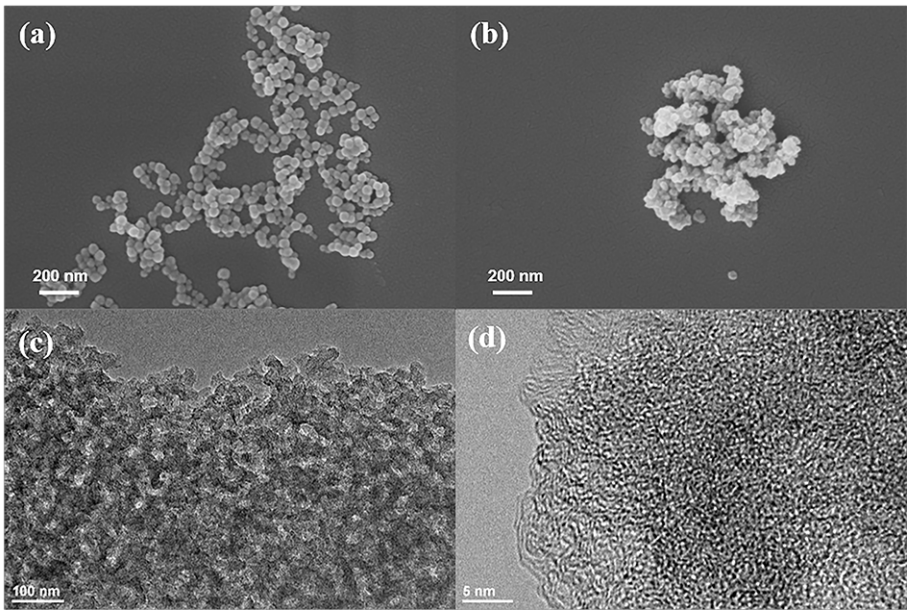

Fig. S13 (a) SEM images of ZnCo(19:1)–ZIF. (b) SEM images of Co–NC. (c, d) TEM and HRTEM images of Co–NC.

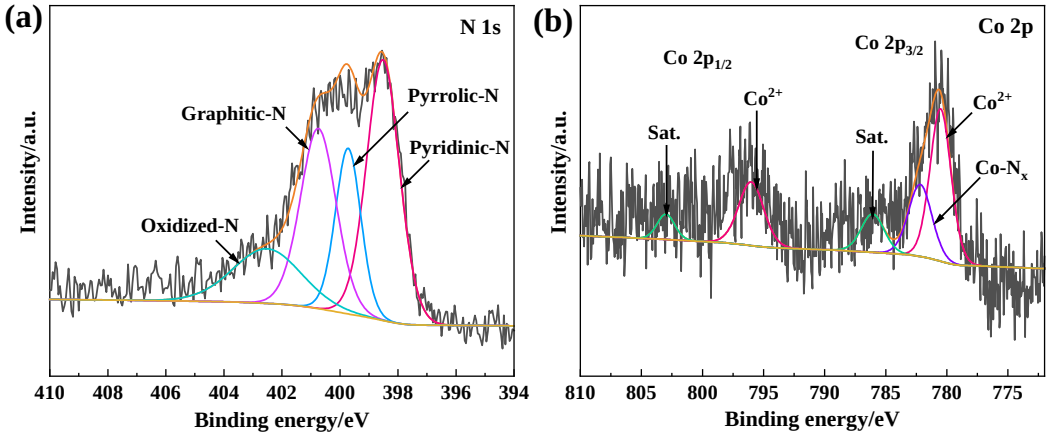

Fig. S14 XPS spectra of (a) N 1s and (b) Co 2p for Co–NC.

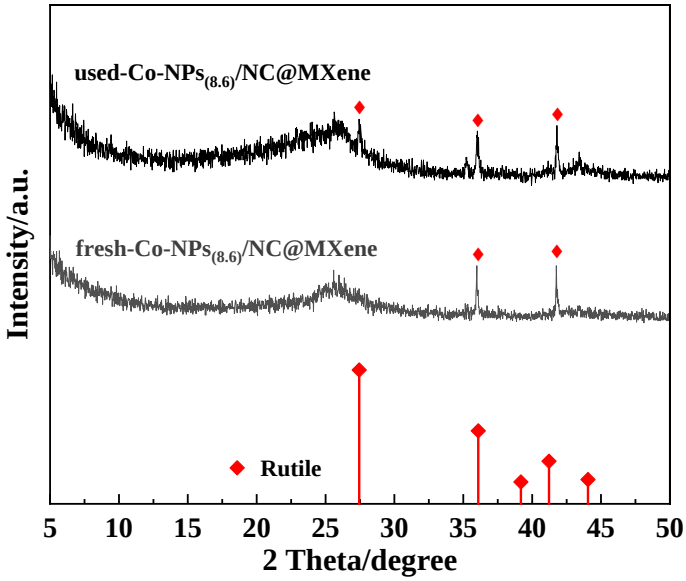

Fig. S15 XRD patterns of fresh and used Co–$NPs_{(8.6)}$/NC@MXene.

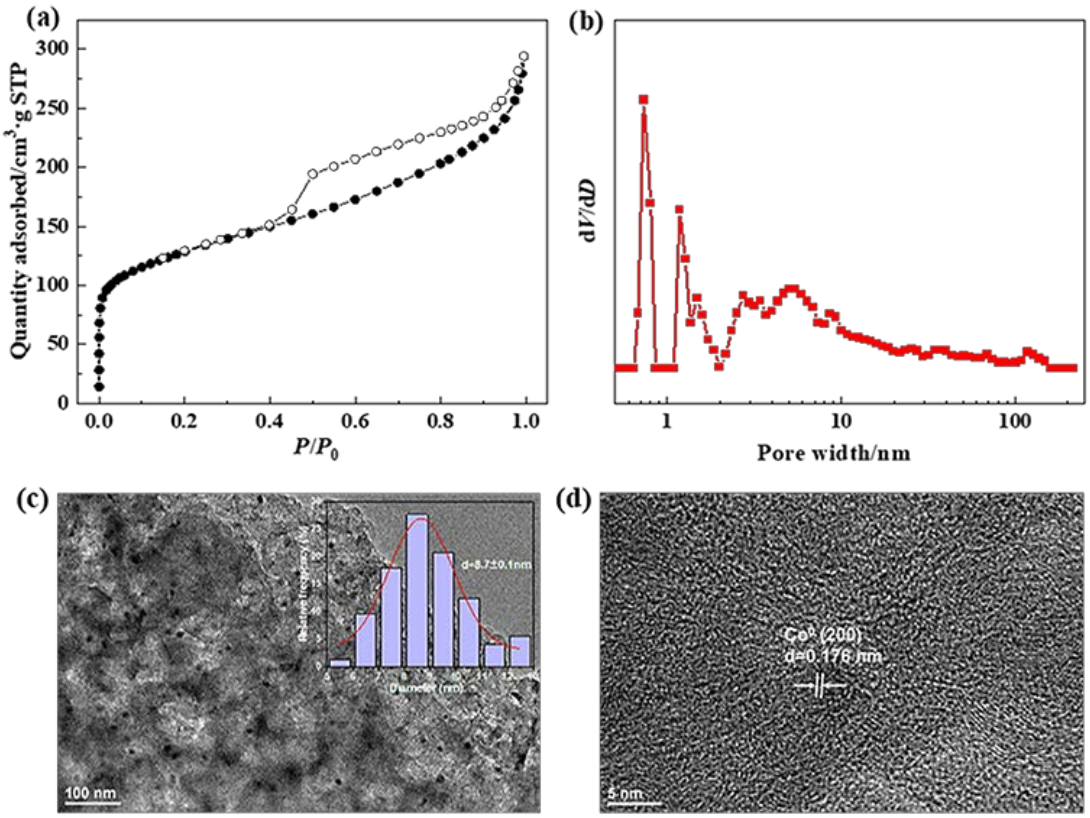

Fig. S16 (a) XRD patterns, (b) N_2 adsorption–desorption isotherms and pore size distribution, and (c, d) TEM and HRTEM images of used Co–$NPs_{(8.6)}$/NC@MXene.

MS spectra of the typical products

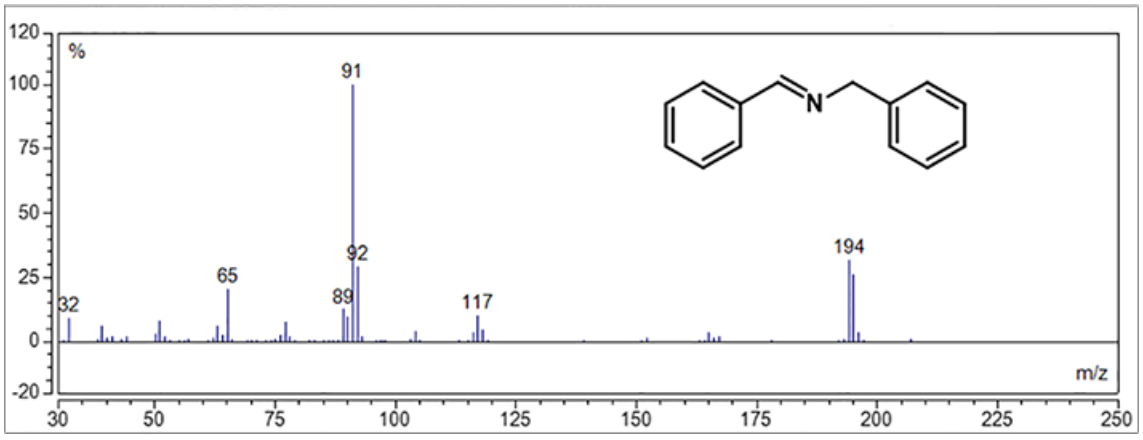

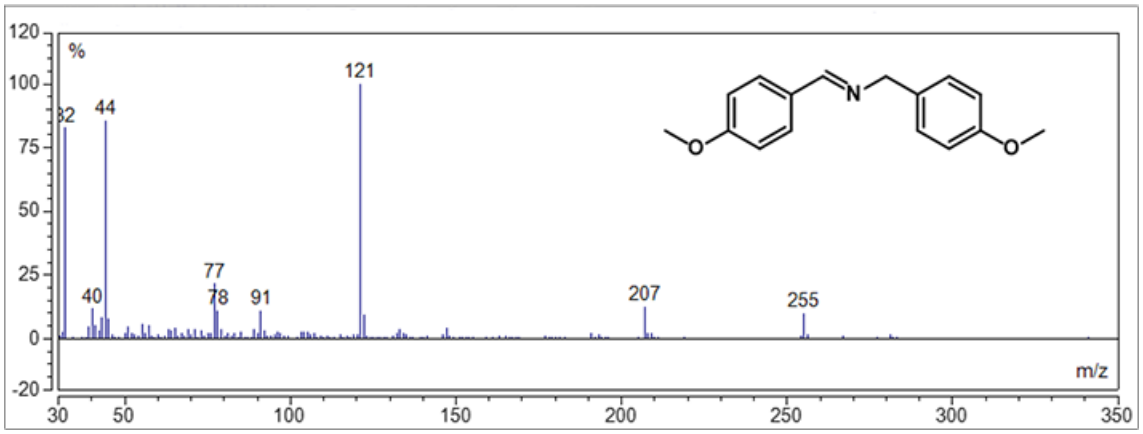
%
121
32
44
77
78
91
40
207
255
m/z
N
O
O

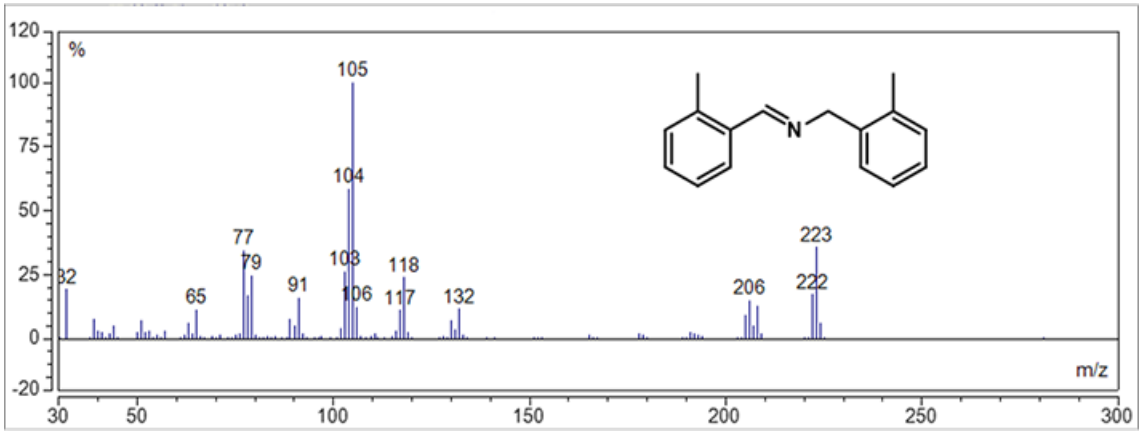
%
105
104
77
79
103
118
91
106
117
132
65
32
206
223
222
m/z
N

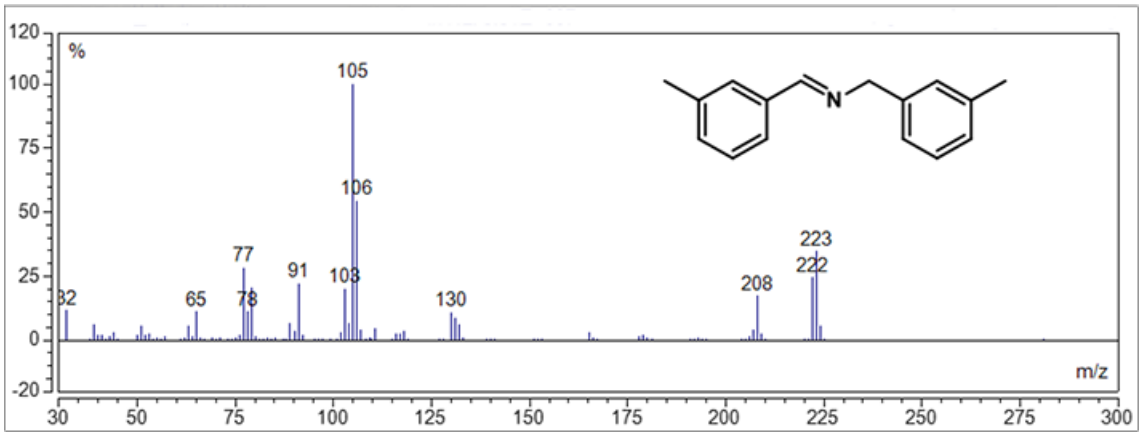
%
105
106
77
91
103
65
78
130
32
208
223
222
m/z
N

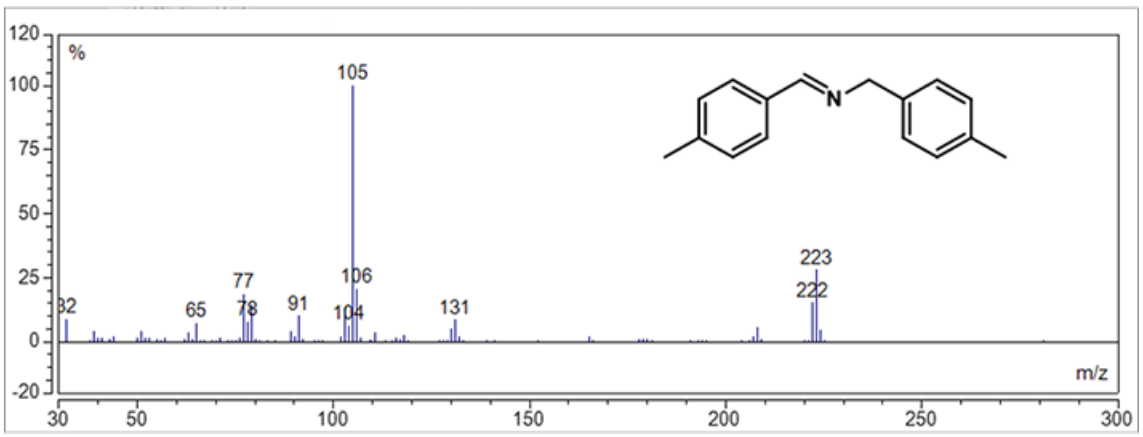
%
105
106
77
91
104
65
78
131
32
223
222
m/z
N

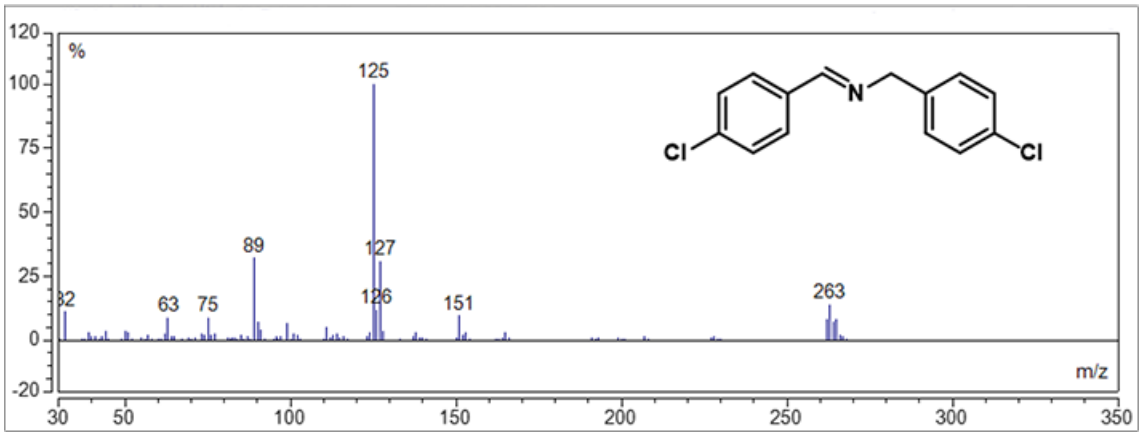
%
125
89
127
126
151
263
32
63
75
Cl
Cl
N
m/z

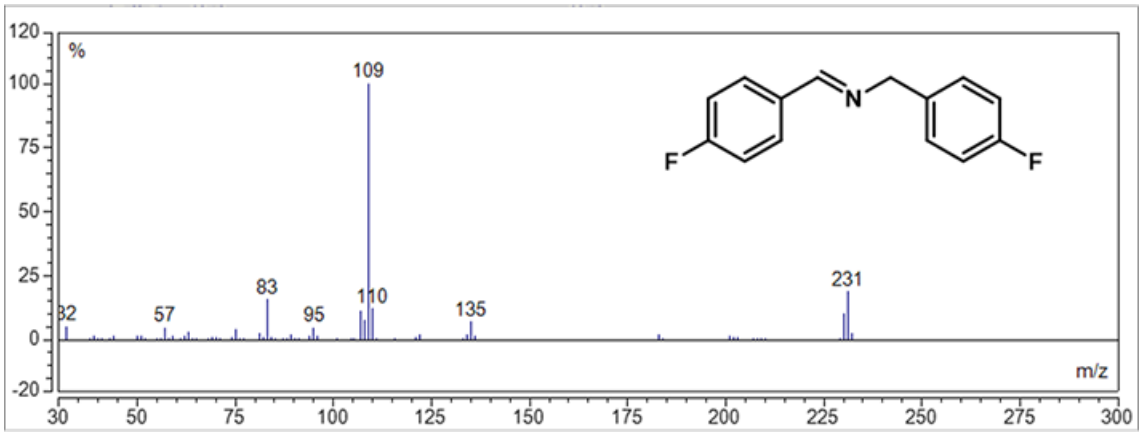
%
109
83
110
135
231
32
57
95
F
F
N
m/z

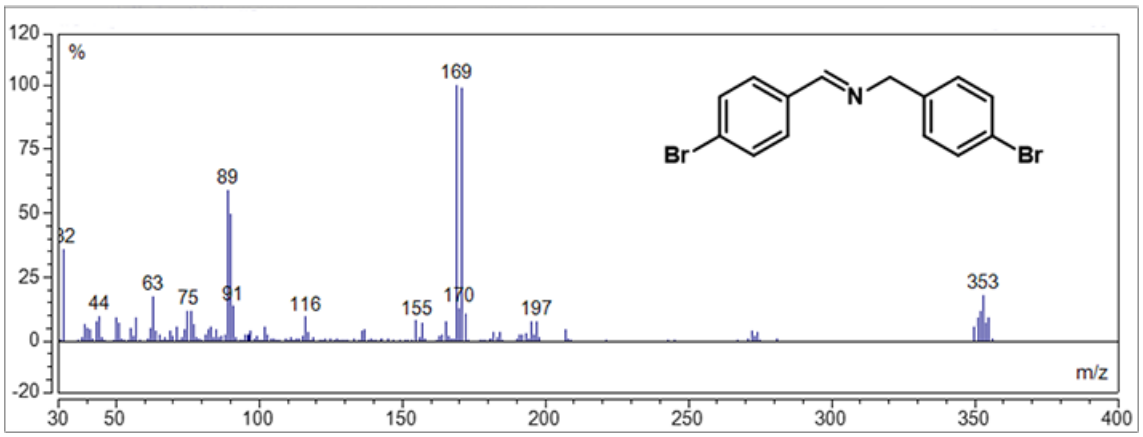
%
169
89
32
63
75
91
44
116
155
170
197
353
Br
Br
N
m/z

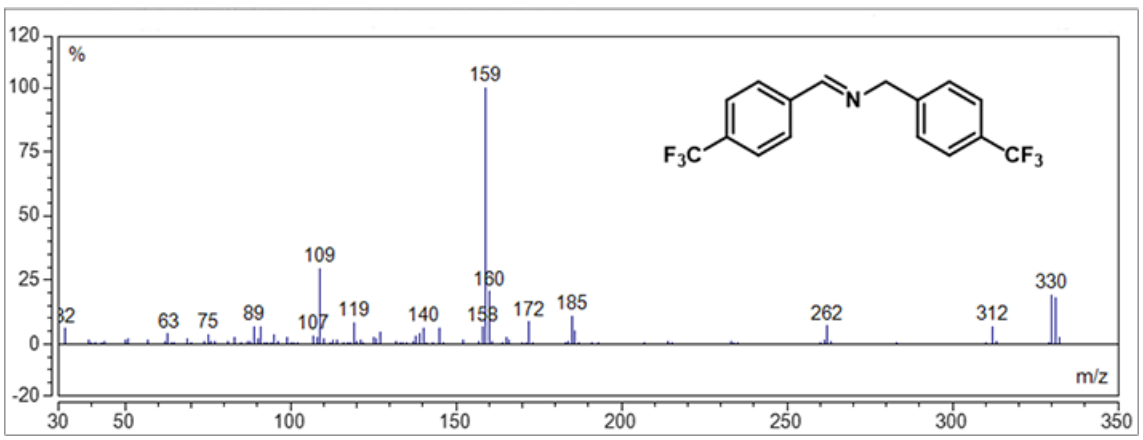
%
159
109
160
119
140
158
172
185
262
312
330
32
63
75
89
107
F3C
CF3
N
m/z

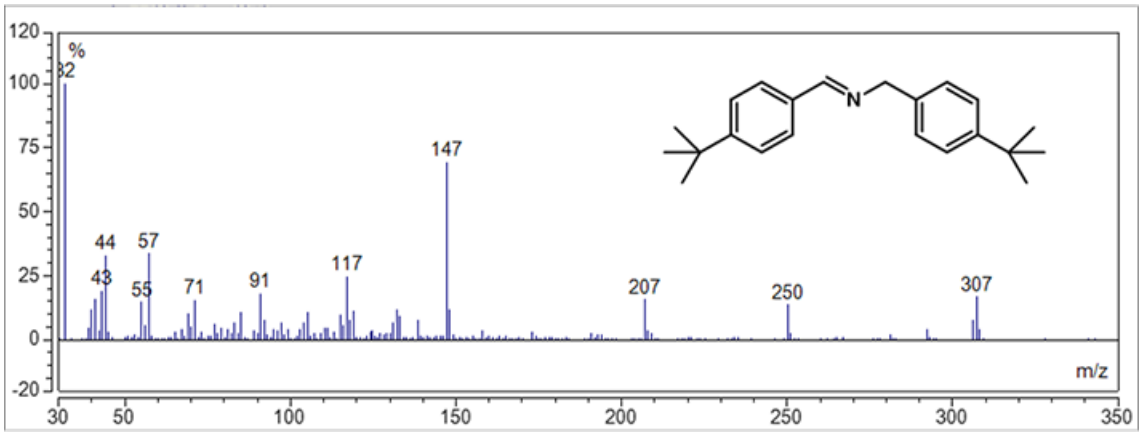
%
32
147
44
57
43
55
71
91
117
207
250
307
m/z
N

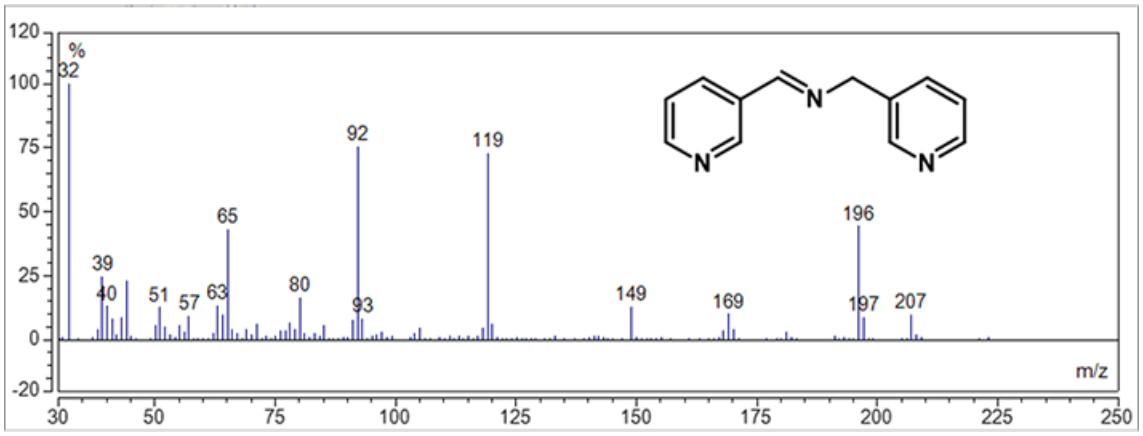
%
32
92
119
65
196
39
40
51
57
63
80
93
149
169
197
207
m/z
N
N
N

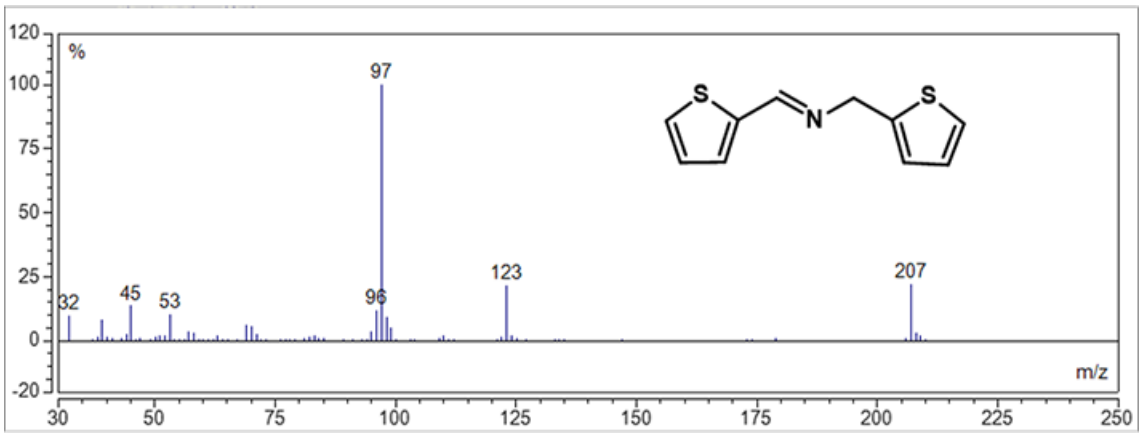
%
97
32
45
53
96
123
207
m/z
S
N
S

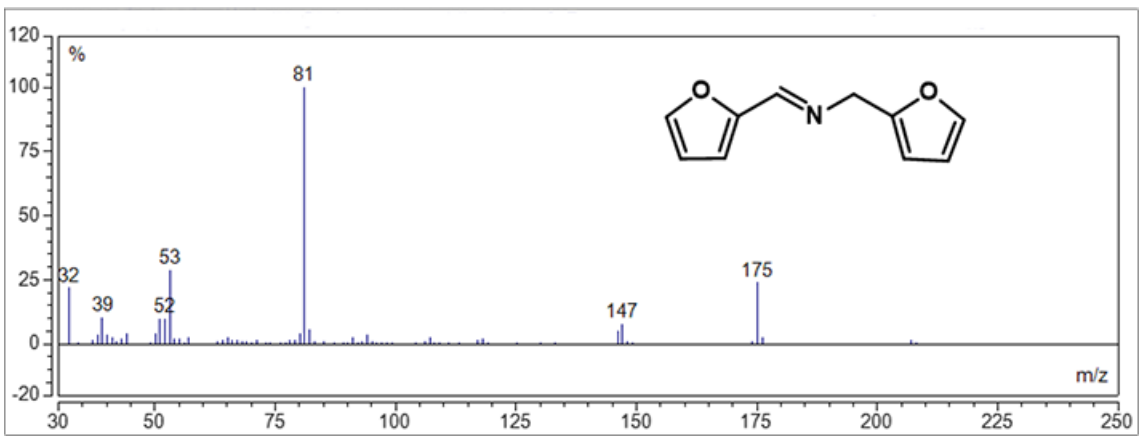
%
81
32
53
39
52
147
175
m/z
O
N
O

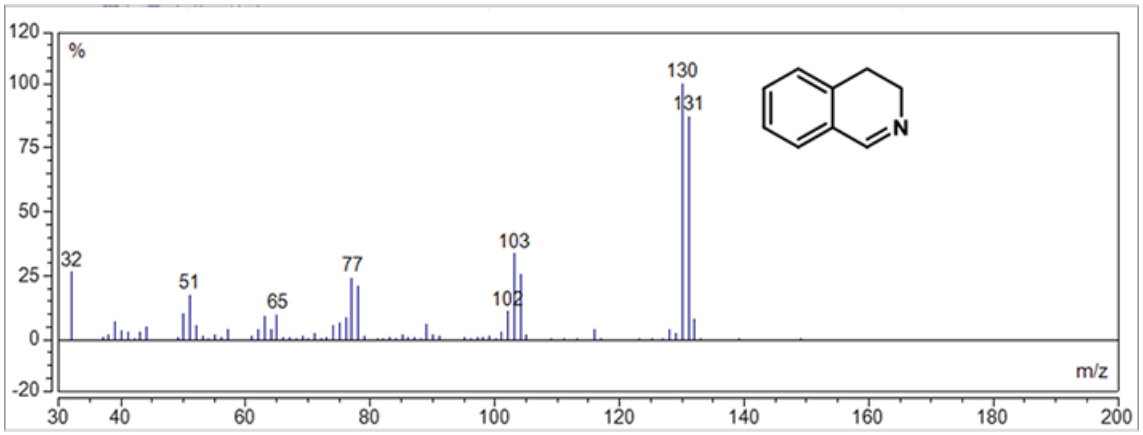

MS spectra of the intermediates

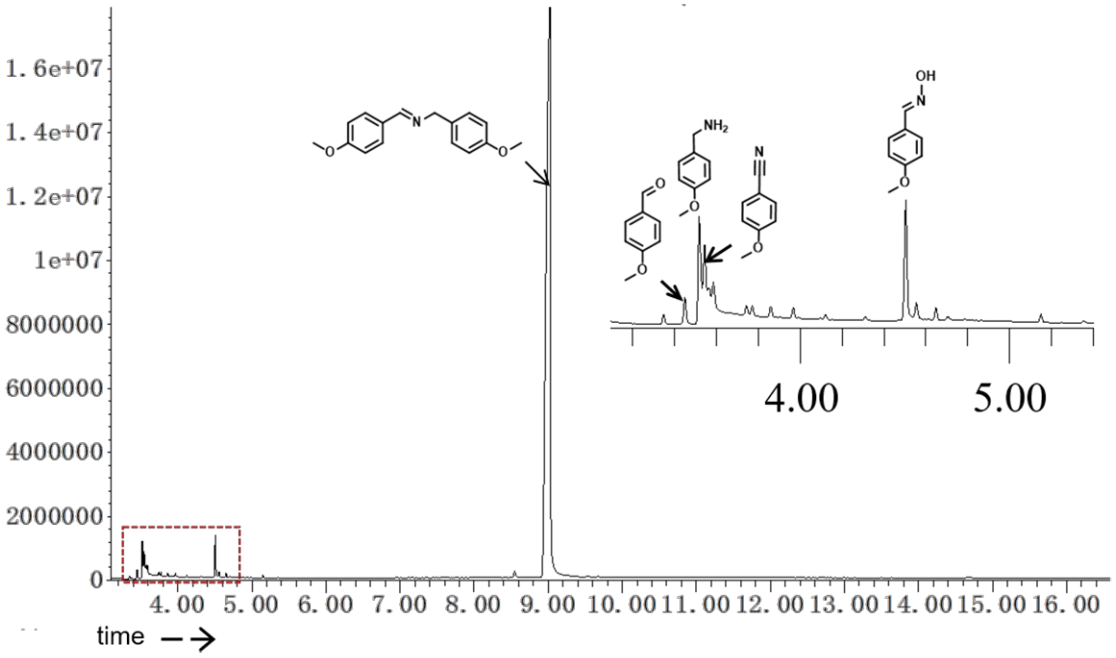

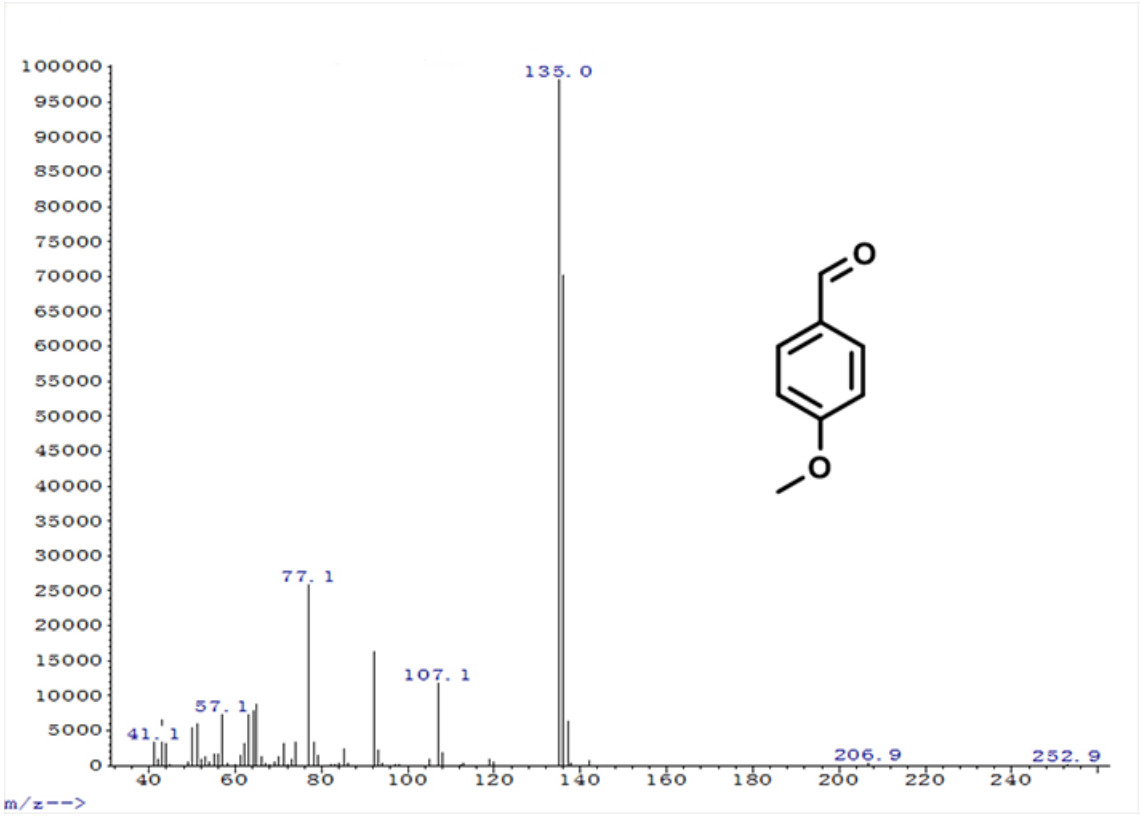
135.0
77.1
107.1
57.1
41.1
206.9
252.9
m/z-->

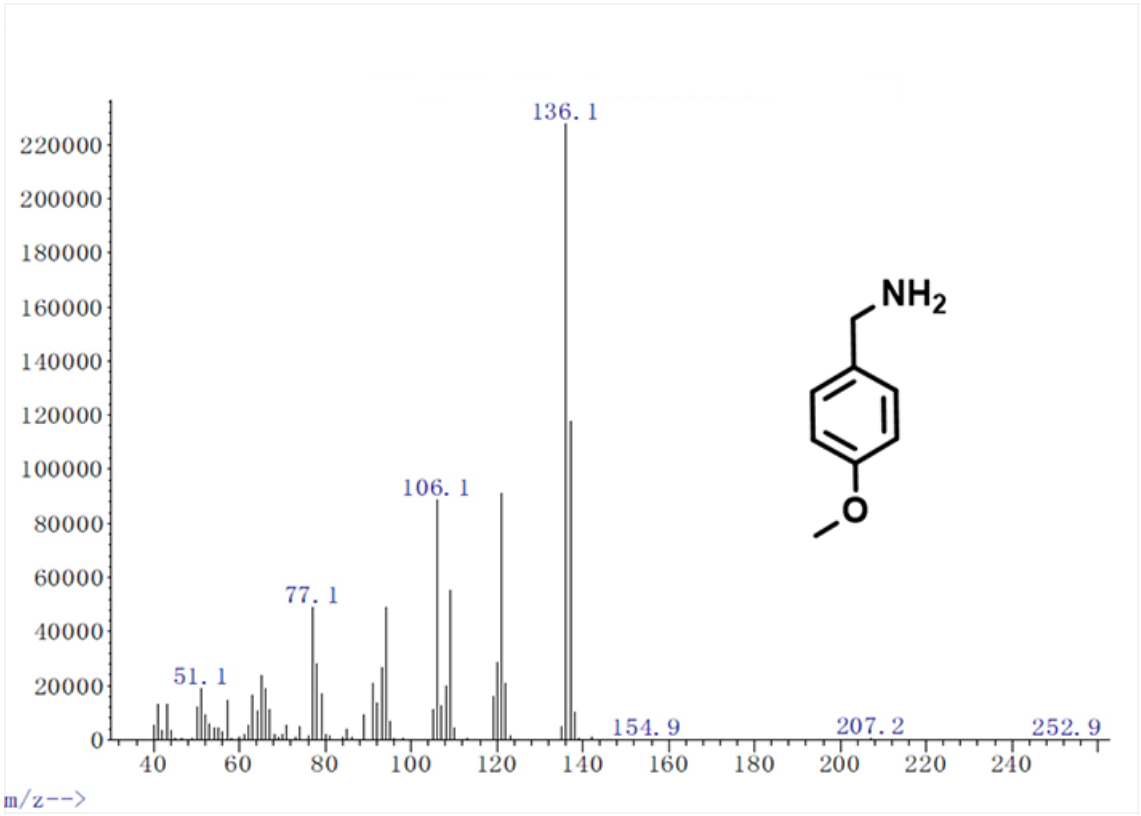
136.1
106.1
77.1
51.1
154.9
207.2
252.9
NH2
m/z-->

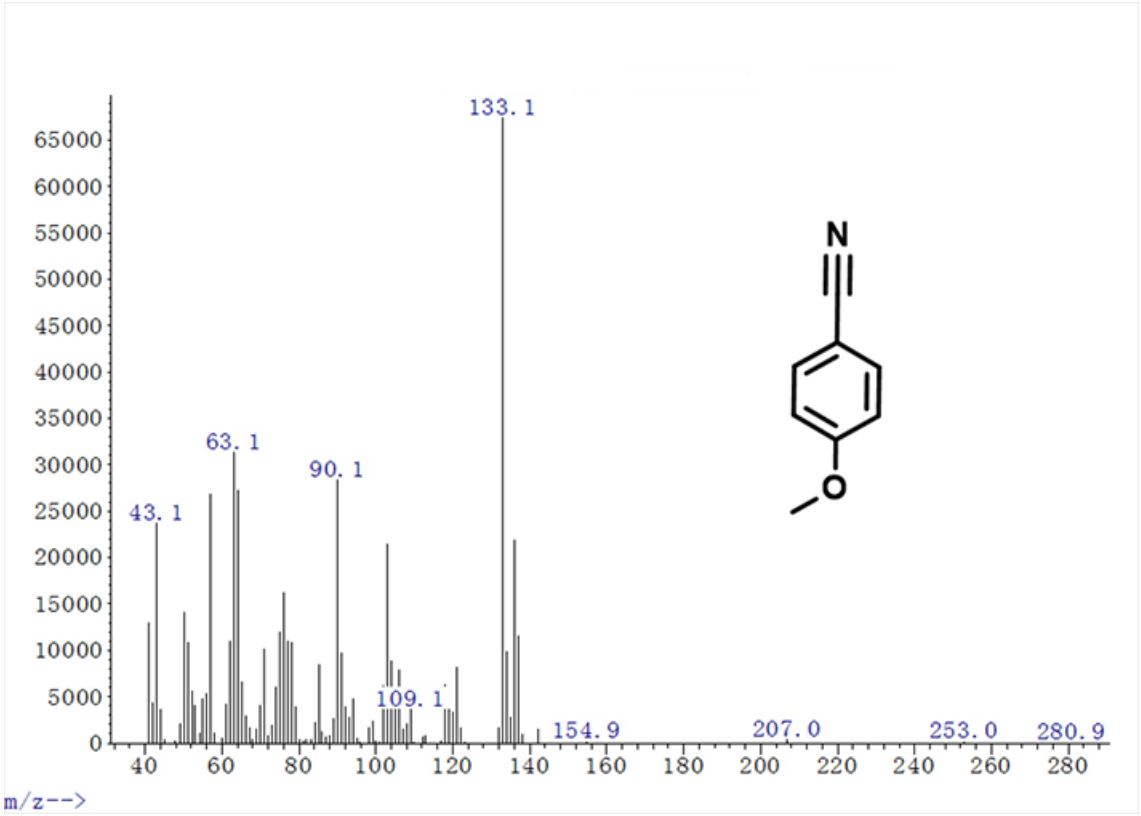
133.1
63.1
90.1
43.1
109.1
154.9
207.0
253.0
280.9
N
O
m/z-->

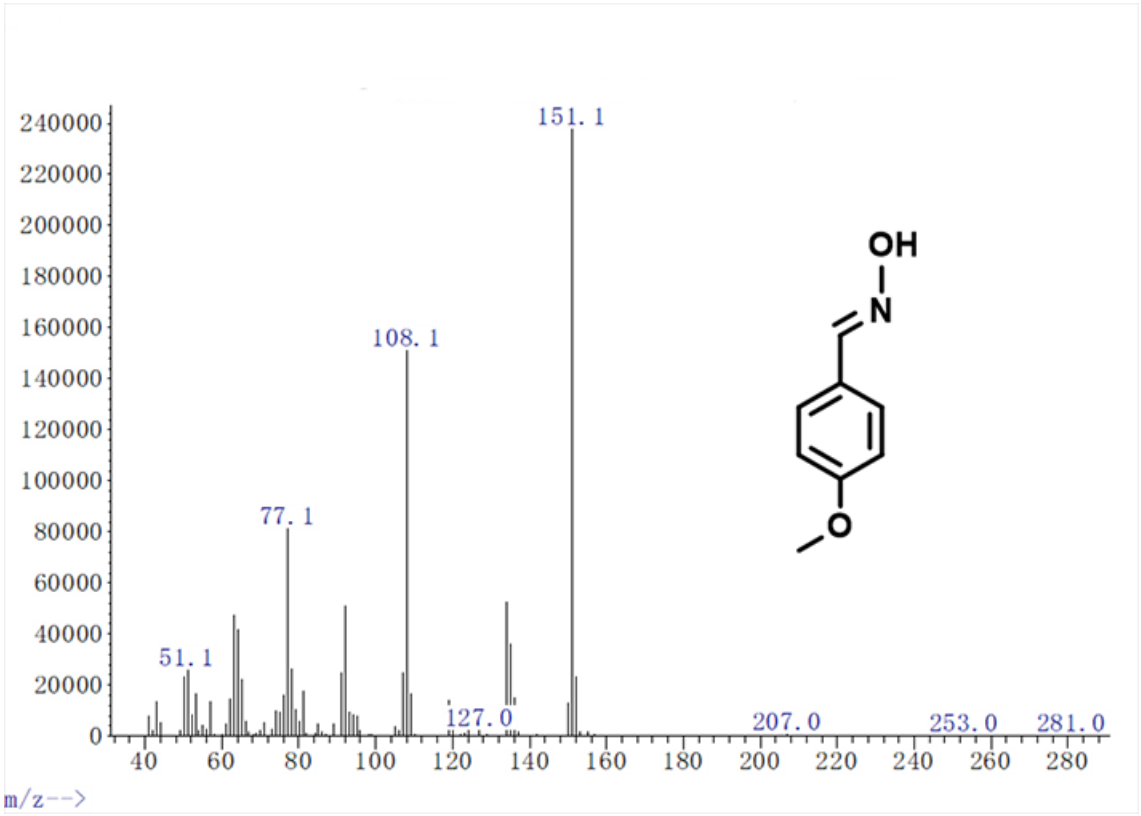
151.1
108.1
77.1
51.1
127.0
207.0
253.0
281.0
OH
N
O
m/z-->